NUREG/CR-2848
LA-9460-MS

Mechanistic Dry-Pressure-Containment LOCA Analysis

Prepared by R. Gido, D. Lamkin, A. Koestel

Los Alamos National Laboratory

**Prepared for
U.S. Nuclear Regulatory
Commission**

GPO Printed copy price: $4.75

NUREG/CR-2848
LA-9460-MS
R4

Mechanistic Dry-Pressure-Containment LOCA Analysis

Manuscript Completed: June 1982
Date Published: January 1983

Prepared by
R. Gido, D. Lamkin, A. Koestel*

Los Alamos National Laboratory
Los Alamos, NM 87545

*Consultant

Prepared for
Division of Systems Integration
Office of Nuclear Reactor Regulation
U.S. Nuclear Regulatory Commission
Washington, D.C. 20555
NRC FIN A7105

CONTENTS

NOMENCLATURE AND DIMENSIONS

A	surface area	m^2
B	wave or roughness height	m
b	wave height	m
C	mass concentration per unit volume	kg/m^3
$\hat{C}$	drop mass concentration at peak velocity	kg/m^3
c_R	velocity of propagation of a disturbance wave relative to the undisturbed fluid that may be moving at some uniform velocity	m/s
D	diffusivity; tube or equivalent diameter	m^2/s; m
D_d	Brownian drop mass diffusivity	m^2/s
DMDE	condensed mass per unit of energy transfer	kg/J
d	drop diameter	m
f	ratio of bulk air to steam mass	none
f'	superficial friction factor, i.e., based on superficial velocity	none
g	gravitational acceleration	m/s^2
$\bar{H}$	mean vertical wall height	m
h	enthalpy	J/kg
h_c	condensing heat transfer coefficient	$W/m^2/K$
h_f	saturated liquid enthalpy	J/kg
h_{fg}	latent heat of vaporization/condensation	J/kg
h_g	saturated vapor enthalpy	J/kg
K	universal constant used to define Prandtl mixing length for turbulent flow	none
K'	Boltzmann's constant	$kg \cdot m^2/s^2/K$

ℓ	Prandtl mixing length	m
m	mass flow rate per unit area	kg/m^2
S	constant	none
T	absolute temperature	K
u	velocity	m/s
$\hat{u}$	peak velocity	m/s
u'	mean turbulent velocity fluctuation	m/s
u_c	wave crest (celerity) velocity	m/s
u_δ	mean film velocity	m/s
u_t	terminal velocity	m/s
V_*	interfacial shear stress or friction velocity, $\sqrt{\tau/\rho}$	m/s
V_+	dimensionless particle (drop) deposition velocity	none
V'	superficial or far from wall, e.g., mean bulk, velocity	m/s
x	quality or vapor fraction	none
y	normal-to-wall coordinate	m
$\hat{y}$	y coordinate at peak velocity	m

Greek

α	ratio of steam mass to that condensed	none
β	mass-transfer coefficient	m/s
β_d	drop mass-transfer coefficient	m/s
Γ	average mass rate of liquid flow per unit width of wetted wall	kg/s/m

NOMENCLATURE AND DIMENSIONS (cont)

δ	mean film thickness	m
δ_B	minimum wave thickness	m
Δ	boundary layer thickness	m
ΔT	temperature difference	K
ε	momentum eddy diffusivity	m^2/s
ε_d	drop mass eddy diffusivity	m^2/s
μ	viscosity	$N \cdot s/m$
ν	kinetic or dynamic viscosity = μ/ρ	m/s^2
ρ	density	kg/m^3
τ	shear stress	N/m^2
T	particle relaxation time	s

Subscripts

a	air
avg.	average
b	bulk
c	wave crest or nearby region, condensing
d	drop
δ	at δ location, or mean thickness, of liquid film
g	gas
in	inlet value
ℓ	liquid
s	steam
w	wall or near wall location

MECHANISTIC DRY-PRESSURE-CONTAINMENT LOCA ANALYSIS

by

R. Gido, D. Lamkin, and A. Koestel

ABSTRACT

Procedures for performing mechanistic dry-pressure-containment LOCA analyses are presented, evaluated, applied, and compared with other approaches. The procedures are based on (1) the blowdown-introduced small drops (10 to 100 μm) being homogeneously mixed into the atmosphere, (2) drop (particle) turbulent deposition on vertical surfaces, and (3) terminal velocity gravity deposition on the floor. Variation of drop size and mass transfer deposition velocity was found to have a small effect on calculated results, except for the atmosphere water mass retention. The primary effect of the mechanistic approach was a saturated containment atmosphere, with significant atmosphere water retention. The calculated containment pressure of the mechanistic approach was lower, before the spray initiation, than that calculated by other current procedures.

I. INTRODUCTION

The purpose of this report is to introduce and evaluate the effect of a mechanistic approach to the containment analysis of a loss-of-coolant accident (LOCA). The physical processes involved in the transfer of LOCA blowdown water to the containment sump are central to this study. Because approximately 60% of the blowdown is saturated water, different assumptions regarding the introduction of the phases into the containment have been made. For example, Ref. 1 considers the possibility that the break flow is partitioned into separate liquid and vapor phases. The liquid is assumed to go directly to the sump whereas the vapor phase is introduced into the containment vapor-air volume for the determination of pressure and temperature. On the other hand, Ref. 2 introduces the full break flow into the containment, calculates the corresponding equilibrium conditions, and then assumes that any liquid water falls immediately to the sump. In both references, condensed water caused by heat transfer to internal surfaces is also added to the sump. Clearly, different values for the containment pressure, temperature, and atmosphere water content and sump mass and temperature will result from these very different ways of handling the blowdown.

The physical processes by which the blowdown makes its way to the sump are, of course, very complicated.[3] However, several interdependent mechanisms can be identified.

1. Condensation heat transfer.
2. Hydrodynamic interaction between the condensate film and the vapor-air-liquid drop boundary layer.
3. Containment convection currents.
4. Drop deposition resulting from turbulence and gravity.
5. Thermal and aerodynamic liquid fragmentation.
6. Coagulation.

We have investigated these phenomena in some detail over the past several years.[4-8] As a result, we believe that a mechanistic representation of the containment is as shown in Fig. 1. Approximate values of pertinent quantities

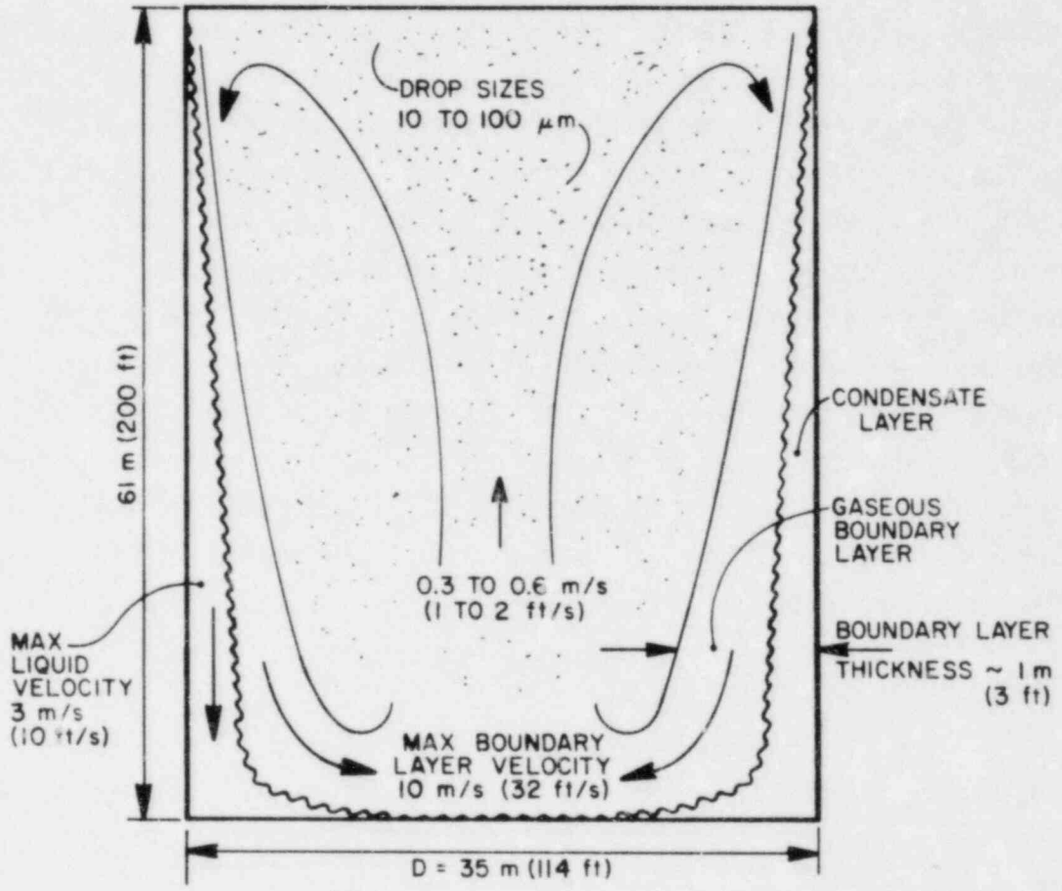

Fig. 1. Mechanistic-containment-approach representation. Kinematic values are caused by the gravity-induced flow pattern where T_{wall} = 300 K (80°F), T_{bulk} = 400 K (260°F), P = 3 bars, and air circulation per hour is ~ 21.

are indicated on the figure to provide a physical perspective. In particular, note that the blowdown has been introduced into the containment atmosphere as a saturated mixture of vapor and small drops. The drops have been estimated to be in the 10-100 μm-size range.[7] Because of their small size, the drops are assumed to be readily maintained in the atmosphere as a uniform dispersion because of the turbulence introduced by the blowdown momenta and the gravity-induced turbulent convection currents.

The physical picture depicted in Fig. 1, which forms the basis of our analysis, indicates a containment control volume of a homogeneous mixture of air, steam, and small liquid water drops. The assumption that a homogeneous mixture exists requires qualification because the mixing of the blowdown, with its small drops, may be restricted by the local geometry near the blowdown and the time required for mixing to occur. Accounting for the distribution of the blowdown into the containment would be difficult and is not treated in this report. However, Ref. 3 has qualitatively investigated possible mixing mechanisms and their response times to evaluate the degree of mixing that might be expected. That study also concludes that the containment atmosphere will be predominantly a homogeneous mixture. Another way of viewing our assumption is to consider the inclusion of the small drops to be an extrapolation of the current containment analysis procedures.[1,2] The current approaches make the homogeneous control volume assumption but do not consider the blowdown water to be suspended as small drops.

II. METHOD OF ANALYSIS

In this section, the bases for the calculated results presented in Sec. III will be established. In particular, Sec. II.A summarizes the basis for the LOCA blowdown being in the form of a saturated vapor and small drops. Sections II.B and C develop the procedures for calculating the drop-mass transfer to the containment surfaces by assuming that the controlling mechanisms are turbulent deposition (Sec. II.B) and gravity deposition (Sec. II.C). Section II.D discusses other models for the introduction of the blowdown into containment in preparation for the comparisons of calculated containment parameters for all models presented in Sec. III.

A. LOCA-Generated Drop Sizes

Drop sizes of 10-100 μm were estimated to be produced by a LOCA blowdown.[7] The estimates resulted from the consideration of thermal and aerodynamic fragmentation of the liquid bulk as well as coagulation, a process of the opposite character. Thermal fragmentation was determined to be controlling for the temperature levels of a LOCA. Thermal fragmentation results from the vapor

bubbles in the liquid bulk extending the liquid into thin films, which upon rupture leads to the formation of many small drops. Drop sizes were estimated by developing a theoretical thermal fragmentation model that was validated by several sources of experimental measurements for liquid water temperatures up to 422 K ($300^{o}F$). Theory allowed extrapolation to LOCA temperatures. The theoretical treatment required (1) density of potential nucleation sites in the bulk liquid, (2) surface energy formed by bubble growth, (3) the critical condition for "bubble burst," which is an empirical quantity based on several independent test measurements, and (4) conservation of liquid mass and surface energy after bubble burst to compute the drop size.

This discussion describes the basis for the sizes of the LOCA-generated drops that are introduced into the bulk containment. However, within the bulk containment the sizes of the suspended drops might change because of coagulation. The following analyses do not account directly for coagulation because (1) experiments have shown that coagulation is prevented by vapor repulsion while the drops are superheated (Ref. 7, pg. 3), (2) at thermal equilibrium the effect of thermal (Brownian) coagulation can be neglected for the sizes of drops estimated to exist, $> 10\ \mu m$ (Ref. 3, pg. 42), (3) velocity gradient coagulation is neglected because the gradients are predominantly at the containment walls and not in the bulk (Fig. 1), (4) forced coagulation caused by other influences, such as electrical and gravitational, are unknown and therefore neglected, and (5) any drop size variation caused by coagulation is more than accounted for by the drop size variation sensitivity study included in the analysis.

B. Deposition

A convenient starting point for computing drop deposition is to assume that the momentum analogy is applicable, after which limitations can be introduced. Knowledge of the limitations is crucial because one must extrapolate with confidence from what one can gather from small-scale experiments conducted in tubes to large-scale containment conditions, where the hydrodynamics may be markedly different. Research into the subject has shown that the momentum analogy is indeed the basis for computing drop deposition but with many deviating effects, mainly caused by the inertia of the drop. When drops are diffused by turbulence, the inertia of large drops prevents them from following

the turbulent eddies of the vehicle fluid. This causes the eddy kinematic viscosity of the drops to be different from that of the fluid, namely, $\varepsilon_d \neq \varepsilon$. When drops are diffused in the laminar regime, such as in a laminar sublayer adjacent to a wall, it is by Brownian motion where the enormous size of the drops, in contrast to that of the molecules, makes the diffusivity of the drops (D_d) much less than the diffusivity (D) of a diffusing species on a molecular scale (namely, $D_d < D$). The diffusivity of droplets by Brownian motion can be computed by means of Einstein's equation [Eq. (A-2)], which indicates that D_d decreases with drop size and gas viscosity. Einstein's equation accounts for the drop inertia as it diffuses in laminar flow. No such formulation is available for the eddy kinematic viscosity of drops although several analyses have been presented in the literature with varying success in their applications.[9-11] However, there appears to be one common parameter, the meaning of which can be interpreted by means of the relaxation phenomena.[12] The relaxation time, based on Stokes Law, is

$$T = \frac{\rho_\ell \, d^2}{18\mu} \quad , \tag{1}$$

where ρ_ℓ is the liquid drop density, d is the drop diameter, and μ is the surrounding medium viscosity. The relaxation time is a measure of the drop inertia in a turbulent eddy. A normalized nondimensional expression for the relaxation time is presented in the following discussion.

When the deposition mass-transfer coefficient is plotted vs the drop size for a given flow condition, a curve such as depicted in Fig. 2 is obtained. Two distinct regimes are formed. One is diffusion controlled by Brownian motion and the other, by turbulent eddy. Both regimes show a decrease in the mass-transfer coefficient with an increase in drop size caused by inertia. For extremely small particles ($d < \sim 0.1$ μm) the deposition is limited by Brownian motion in the laminary sublayer as computed by Einstein's equation. For particle sizes greater than about 0.1 μm, the turbulence outside the laminar sublayer imparts sufficient momentum to the particles so as to effect their transport through the layer. This describes the transition to the region wherein the laminar sublayer can no longer attenuate the effects of turbulence. In this region of large particle size, the response of the particles

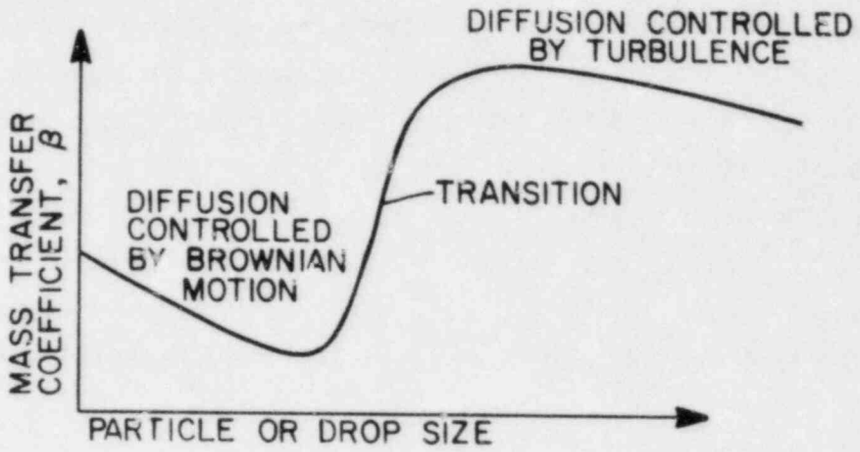

Fig. 2. Mass-transfer coefficient vs drop diameter for a given flow condition in a smooth tube.

to the turbulent fluctuation controls the transfer rate at the wall. Drops of diameters greater than about 50 μm show effects of inertia in that their eddy diffusivity begins to deviate from that of the fluid. The laminar sublayer appears to be irrelevant in the transfer of drops in the turbulence-controlled regime because the turbulence imparted to the drops is readily transmitted to the wall as observed in Ref. 13.

Two effects must be considered when evaluating the role of the laminar sublayer in the transfer of droplets through it. One is the "Stokes' stopping distance" and the other the Staffman lift force.[9,11,14-16] The former is a measure of the inertial coasting effect as a means of transporting drops across the laminar sublayer. The initial inertia is imparted to the drop by the turbulence. The latter is concerned with a force acting on the drop in a direction normal to the wall because of the presence of a steep velocity gradient as in the laminar sublayer. This force can propel the drop either toward the wall or away from the wall, depending on whether the velocity of the drop is greater or less than the local fluid velocity. Again, the inertia of the drop on entering the laminar sublayer determines the direction of the lift force. If the drop velocity is greater than the local fluid velocity, the drop will be deflected toward the wall; otherwise, it will be deflected away from the wall. Both effects mentioned indicate that, if there is sufficient turbulence-induced inertia, the drop can coast or be propelled toward the wall.

Many experimental analysts have correlated their results within a factor of about three with measurement reproducibility of about 50%. However, each

theory presented is applicable within a certain regime as depicted in Fig. 2. If researchers are to extend their work to containment conditions, the regime limits should be evaluated. After searching the literature, we found one outstanding source that provided sufficient generalization for identifying the location of the transition regime. This is important because the droplet mass-transfer coefficient can decrease by several magnitudes when it is limited by Brownian movement. The source is Ref. 12 and Fig. 3 is reproduced from it. This figure correlates the dimensionless particle (drop) deposition velocity

$$V_+ = \frac{\beta}{V_\star} \tag{2}$$

vs the dimensionless relaxation time

$$T_+ = \frac{T\, V_\star^2}{\nu} \quad , \tag{3}$$

where β is the mass-transfer coefficient (also called the deposition velocity), $V_\star = \sqrt{\tau/\rho}$ the shear stress velocity, τ is the surface shear stress, ρ is the fluid (not the liquid) density near the surface, T is given by Eq. (1), and ν is the fluid kinematic viscosity.

An advantage of the Ref. 12 correlation is that a monodispersion of drops was used, which provided better control of variables. Drop sizes ranged from about 1 μm to 25 μm, and four other independent sources of data were included in the correlation. However, as pointed out in Appendix A, the falling liquid film formed during a LOCA will be turbulent with a "rough" interface, thereby causing the entire gas boundary layer to be in the turbulent regime. Without a laminar sublayer to impede the transfer of droplets, the transition regime to Brownian movement needs no further consideration.

Note that in Fig. 3 the quantity V_+ relates, by analogy, the deposition-transfer coefficient β to the shear stress velocity $V_\star$ as determined by the interfacial hydrodynamics of the falling film. The quantity T_+ accounts for the drop inertia in the turbulent eddies. Although deposition rates can be calculated directly by means of Fig. 3, a supporting deposition analysis was formulated for a typical mechanistic model. Appendix A contains the analysis, which provides support to the upper values of V_+. In addition, the estimated drop sizes of 10-100 μm (Sec. II.A) result in values of the dimensionless

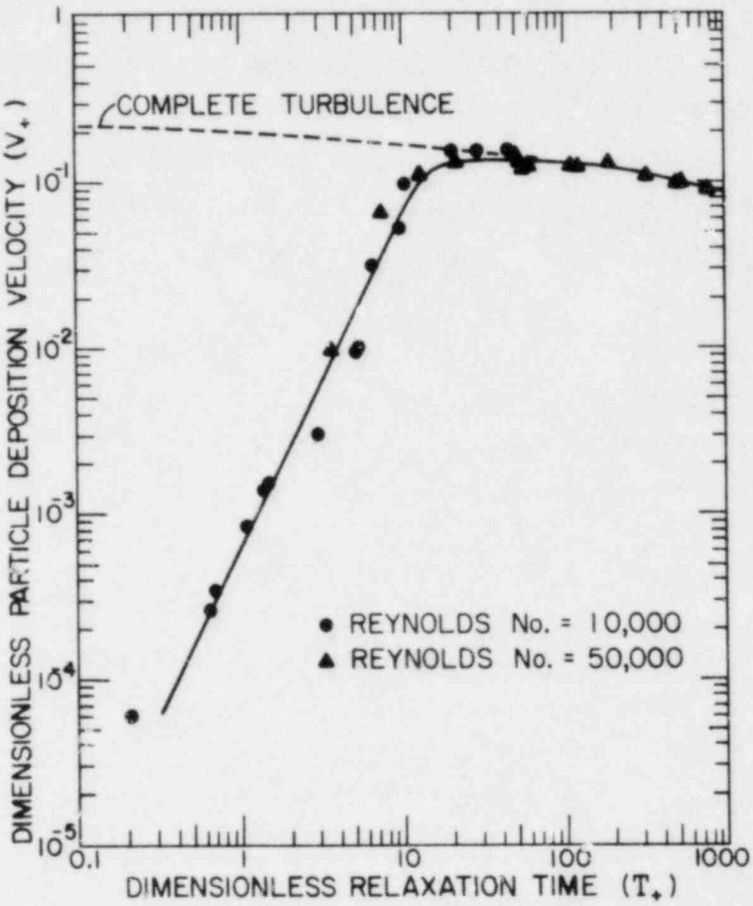

Fig. 3. Experimental relationship between the dimensionless particle deposition velocity and the dimensionless particle relaxation time.[12] (Reprinted with permission from the Journal of Aerosol Science, Volume 5, Benjamin Y. H. Liu and Jugal K. Agarwal, "Experimental Observation of Aerosol Deposition in Turbulent Flow," Copyright 1974, Pergamon Press, Ltd.

relaxation time, T_+, which indicate the applicability of dimensionless particle deposition rates, V_+, near the upper regions of the curve.

C. Shear Stress Velocity

A key parameter required to apply Fig. 3 is the shear stress velocity $V_\star$. A relationship to define $V_\star$ for a falling liquid film is developed in Appendix B. It is

$$V_* \simeq \frac{u_\delta}{10} \quad , \tag{4}$$

where u_δ is the mean velocity of the falling film. The development is based on detailed film measurements presented in Ref. 17 and confirmed by the application of classical hydrodynamic theory.

The use of Eq. (4) requires a value for the mean liquid velocity u_δ. This was obtained by writing a simple balance between the gravitational and shear forces on the falling liquid, which results in the expressions (e.g., see Ref. 18)

$$u_\delta = 1.04(g\nu_\ell)^{1/3}\left(\frac{\Gamma}{\mu_\ell}\right)^{2/3} \quad \text{(laminar)} \quad ,$$

$$u_\delta = 3.73(g\nu_\ell)^{1/3}\left(\frac{\Gamma}{\mu_\ell}\right)^{5/12} \quad \text{(turbulent)} \quad , \tag{5}$$

where g is the gravitational acceleration and Γ is the mean mass rate of liquid flow per unit width of wetted wall. The mass represented by Γ includes that caused by both the condensation and mass transfer.

The film liquid caused by condensation heat transfer is determined from

$$m_c = h_c \, \Delta T \, \bar{H}(DMDE) \quad , \tag{6}$$

where h_c is the heat-transfer coefficient, ΔT is the temperature difference used to calculate the heat transfer, $\bar{H}$ is a mean vertical height, and DMDE is the condensed mass to be associated with the heat transfer. The coefficients used in Eq. (6) are based on the well-known Tagami/Uchida data.[19,20] These coefficients must account for the energy transfer resulting from condensation and the energy transfer from the bulk atmosphere to the vapor-air-liquid drop boundary layer. Therefore, the DMDE term is not the inverse of the latent heat of vaporization/condensation ($1/h_{fg}$) as one might guess. Instead, an expression[8] should be used, i.e.,

$$DMDE = 1./[\alpha f(h_{ba} - \bar{h}_a) + (\alpha - 1)(h_{bs} - \bar{h}) + (h_{bs} - h_\ell)] \quad , \tag{7}$$

where α is the ratio of steam mass entering the boundary layer to that condensed;

f is the ratio of atmosphere (bulk) air to steam mass (a known quantity); h_{ba} and h_{bs} are the bulk atmosphere air and steam enthalpies, respectively; $\bar{h}_a$ and $\bar{h}_s$ are the average boundary layer enthalpies for the air and steam, respectively; h_ℓ is the enthalpy of the condensed liquid assumed to be at the wall temperature. Reference 8 shows that $\alpha \geq 1.0$ and recommends the use of a value of $\alpha = 1.0$ to provide a conservative calculated containment pressure. Conservative in this case is defined to maximize the atmosphere specific internal energy, which provides the potential for maximizing the calculated pressure and temperature. Of course, for a saturated condition only the quality would change.

The Γ terms in Eq. (5) must also include the contribution to the liquid film caused by mass transfer. The drop mass-transfer rate per unit area is

$$m_d = \beta C_b \ , \tag{8}$$

where β is the drop mass-transfer coefficient and C_b is the bulk atmosphere mass concentration (mass/volume). Note that the deposition surface concentration is assumed to be zero, i.e., there are no particles or drops, only liquid. The β term is obtained from the V_+ term of Fig. 3 by

$$\beta = V_+ V_\star = V_+ u_\delta / 10 \ , \tag{9}$$

with u_δ obtained from Eq. (5).

The deposition mass removal from the atmosphere results in an associated energy removal that is based on the enthalpy of liquid water at the atmosphere temperature. We have assumed for convenience that the deposited mass and its associated energy is instantaneously added to the sump. Actually, the deposited mass will be added to the liquid film on the condensing surfaces. The film temperature will increase and cause additional energy transfer to the heat sinks. As a result, the sump temperature will not be as high as our approach provides.

D. Terminal Velocity

Drops introduced into the containment may fall because of gravity. A convenient means of accounting for this precipitation is to use the terminal velocity.

Note that this precipitation would only occur in the lower portions of the containment where the mixing phenomena depicted in Fig. 1 are minimal. However, large heights are not required to achieve terminal velocity for small drops as discussed in Ref. 3. In addition, the assumption of terminal velocity will maximize the calculated deposition caused by gravity. Several equations are available for the calculation of terminal velocity.[21] Using a force balance between gravity and a modified Stokes Law drag (see Ref. 16), the equation we used is

$$\frac{d^2 \rho_\ell g}{18 \mu_g} = u_t \left[1 + 0.15\left(\frac{u_t d}{\nu_g}\right)^{0.687}\right], \tag{10}$$

where d is the drop diameter, ρ_ℓ is the drop density, μ_g is the bulk atmosphere steam-air viscosity, g is the gravitational acceleration force, u_t is the terminal velocity, and ν_g is the bulk atmosphere steam-air mixture kinematic viscosity. This equation was checked by similar equations in Ref. 21 and terminal velocity information given in Ref. 22. Representative values of terminal velocity that result from Eq. (10) at a pressure of 3 bar and temperature of 400 K (260°F) are:

d (μm)	u_t (m/s)	u_t (ft/s)	d (μm)	u_t (m/s)	u_t (ft/)s
1	0.29×10^{-4}	0.94×10^{-4}	100	0.22	0.73
5	0.00073	0.0023	400	1.3	4.2
10	0.0029	0.0094	699	1.9	6.2
40	0.044	0.14	1000	3.0	9.8

Note that we have used the terminal velocity as the deposition velocity on horizontal surfaces.

E. Other Blowdown Models

The mechanistic physical situation depicted in Fig. 1 and calculated by the procedures described in Secs. II.B and C requires comparison with current approaches.[1,2] The current approaches are described in this section to provide basic understanding necessary to assist in understanding the results presented in Sec. III.

The blowdown model of Ref. 2 is based on the assumption that all of the break flow goes into and mixes uniformly with the containment atmosphere. The mixing process results in an air-steam and, possibly, liquid water mixture in thermodynamic equilibrium. After the equilibrium state is reached, a check is made for the existence of liquid water. Any water found is assumed to instantaneously rain to the floor sump. Note that this approach will result in a saturated condition if the blowdown contains a significant quantity of water. However, the rain assumption removes the possibility of previously introduced water acting as a heat sink and thereby prolongs a previous saturated state.

Reference 1 discusses several different models for the partitioning of the blowdown into a vapor part added to the containment atmosphere and a liquid part that is added to the floor sump. The partitioning is based on

$$x = \frac{h_{in} - h_f}{h_g - h_f} \quad , \tag{11}$$

where x is the vapor fraction, h_{in} is the blowdown enthalpy, h_f is the liquid part enthalpy, and h_g is the vapor part enthalpy. The thermodynamic containment conditions for the determination of h_f and h_g in Eq. (11) are varied in Ref. 2. The partition variations are described in Table I. This table provides simple designations for the partition, the instantaneous mixing and the Sec. II.A-D mechanistic models. Note that the Eq. (11) partitioning of the blowdown will result in a superheated atmosphere because only vapor is introduced into the containment control volume.

III. RESULTS

The different methods addressed in Sec. II for performing a containment analysis are evaluated. The evaluation is based on the calculation of containment pressure, temperature, atmosphere water retention, sump water mass, and sump water temperature for a representative dry containment LOCA problem. The representative problem is described in Appendix C, which also discusses the manner of using the COMPARE-Mod 1[23] code for the calculations.

All calculations were performed to the time of spray initiation, which is 60 s for the representative problem. After the time of spray initiation, the mechanistic approach method becomes academic in the sense that the spray water

TABLE I

CONTAINMENT ANALYSIS METHODS

Designation	Partitioning Basis[a] h_g Based on	h_f Based on	Comments
P-P	Total Pressure	Total Pressure	See Eq. (11)
S-P	Steam Partial Pressure	Total Pressure	See Eq. (11)
S-S	Steam Partial Pressure	Steam Partial Pressure	See Eq. (11)
T-T	Temperature	Temperature	See Eq. (11)
I-R	NA	NA	Instantaneous Mixing with Rain
M	NA	NA	Mechanistic

[a] $x = \frac{h_{in} - h_f}{h_g - h_f}$.

drops dominate the containment thermodynamics and the addition of water and energy to the sump. This is due to the relatively large spray drop sizes (100-500 μm, Ref. 3) and the large mass introduced. To facilitate the discussion of the calculated results, the designations for the different methods presented in Table II will be used.

Representative calculated results for the different approaches are presented in Table II and in Figs. 4-6. The Table II calculated results are at 20 and 60 s. Results at 20 s are significant because blowdown is essentially complete at this time (see Appendix C) and is therefore the end of the introduction of water into the atmosphere. Also, after 20 s, many of the parameters, particularly pressure and temperature, do not change much (see Figs. 4-6).

Representative results for the different approaches are given in Table II for convenience. Variations around these representative results have been studied, and the effects of the following variations are presented.

TABLE II

REPRESENTATIVE RESULTS SUMMARY

Approach	Atmosphere				Sump	
	Pressure MPa (psia)	Temp K (°F)	Sat. Temp K (°F)	Water Mass Fraction	Mass Mg (10^5 lbm)	Temp K (°F)
At 20 s						
Instantaneous Mixing with Rain (I-R)	0.384 (55.7)	402 (264)	402 (264)	0.	129 (2.85)	378 (220)
Partition Model (S-P)	0.386 (56.0)	436 (325)	401 (262)	0.	138 (3.04)	397 (254)
Mechanistic Model (M) - V_+ = 0.2, d = 100 μm	0.368 (53.3)	400 (260)	400 (260)	0.39	27 (0.59)	387 (236)
At 60 s						
Instantaneous Mixing with Rain (I-R)	0.397 (57.6)	412 (284)	403 (265)	0.	0.135 (2.98)	375 (215)
Partition Model (S-P)	0.383 (55.4)	432 (319)	400 (260)	0.	0.146 (3.21)	396 (253)
Mechanistic Model (M) - V_+ = 0.2, d = 100 μm	0.376 (54.5)	401 (262)	401 (262)	0.26	0.078 (1.71)	393 (248)

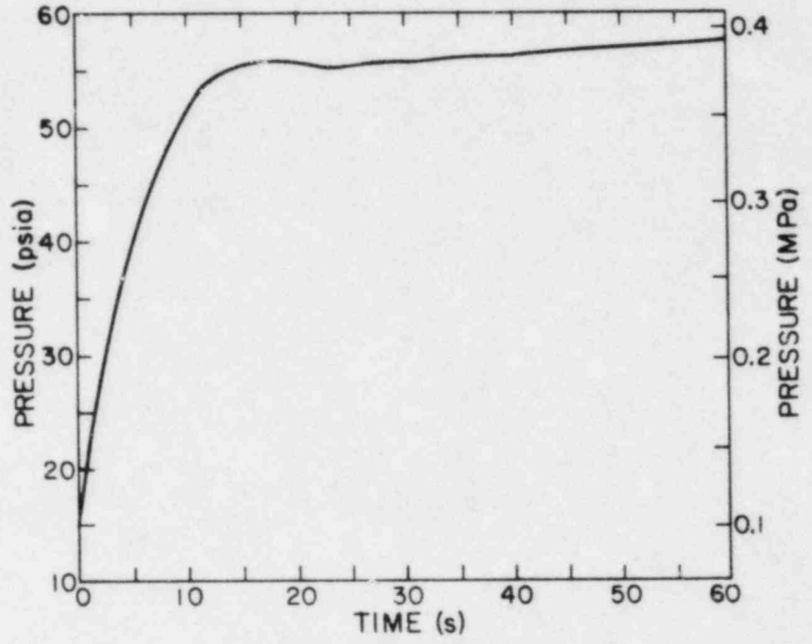

Fig. 4a. Instantaneous mixing approach (I-R) results - Pressure vs Time.

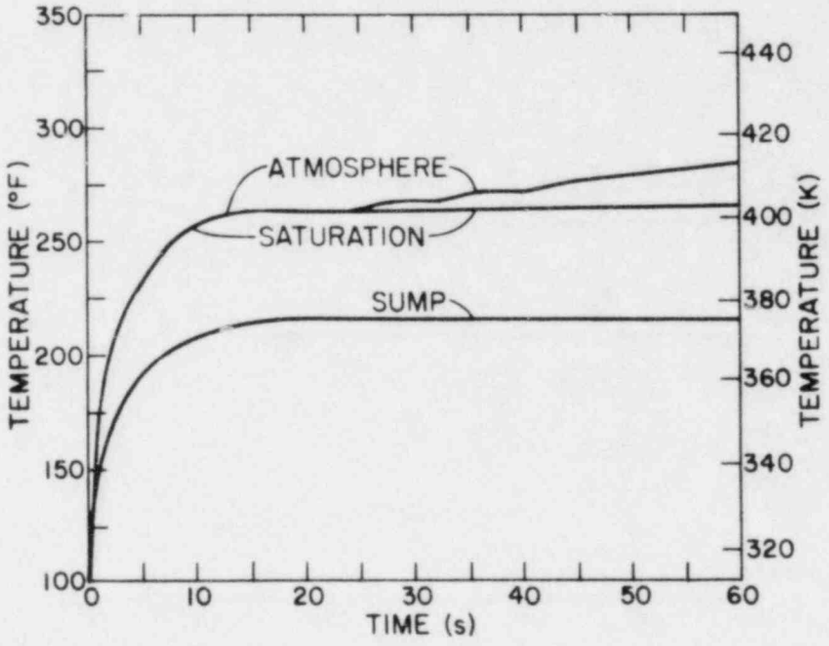

Fig. 4b. Temperature vs Time.

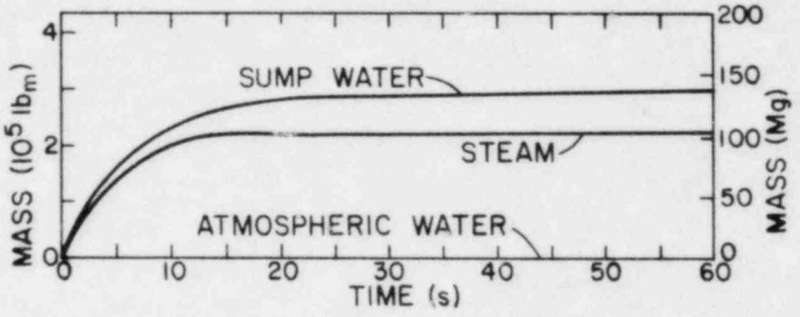

Fig. 4c. Water mass distribution vs time.

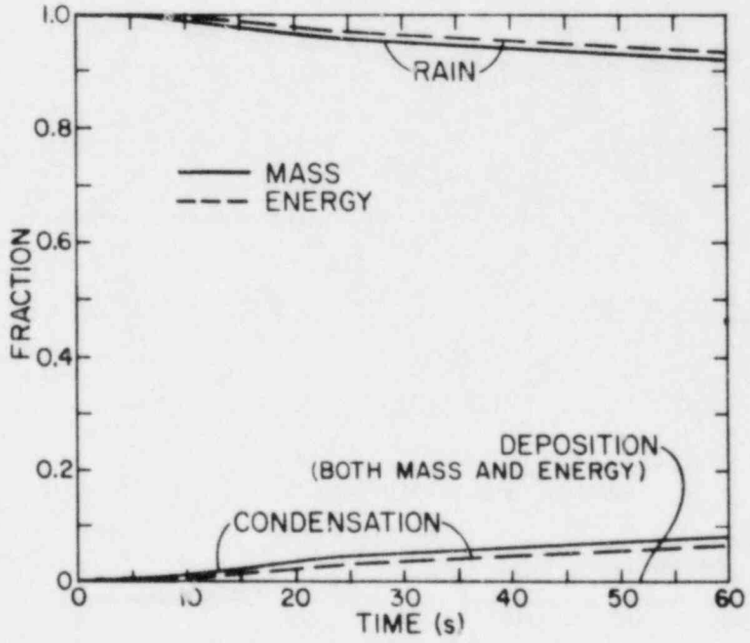

Fig. 4d. Sump mass and energy contribution fractions vs time.

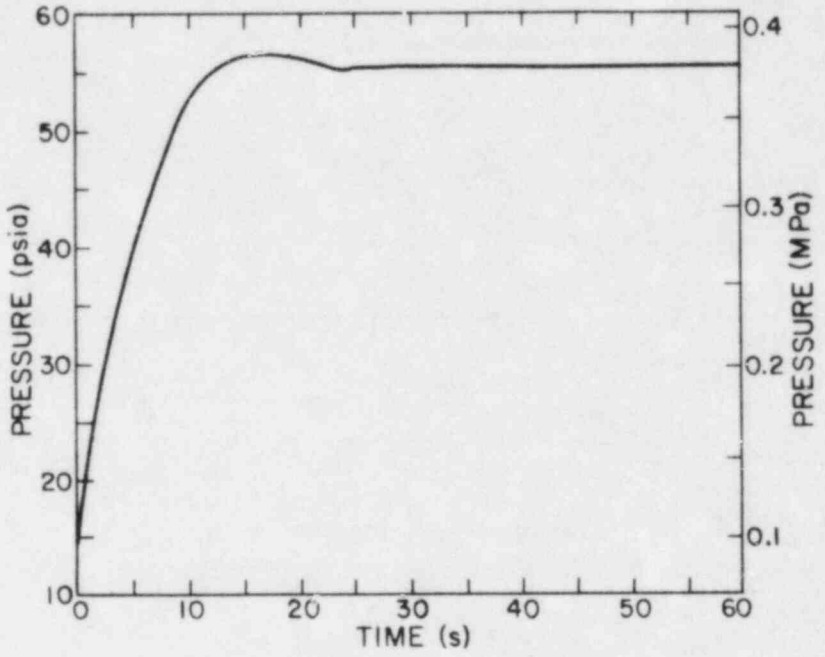

Fig. 5a. Partition model (S-P) calculated results - Pressure vs Time.

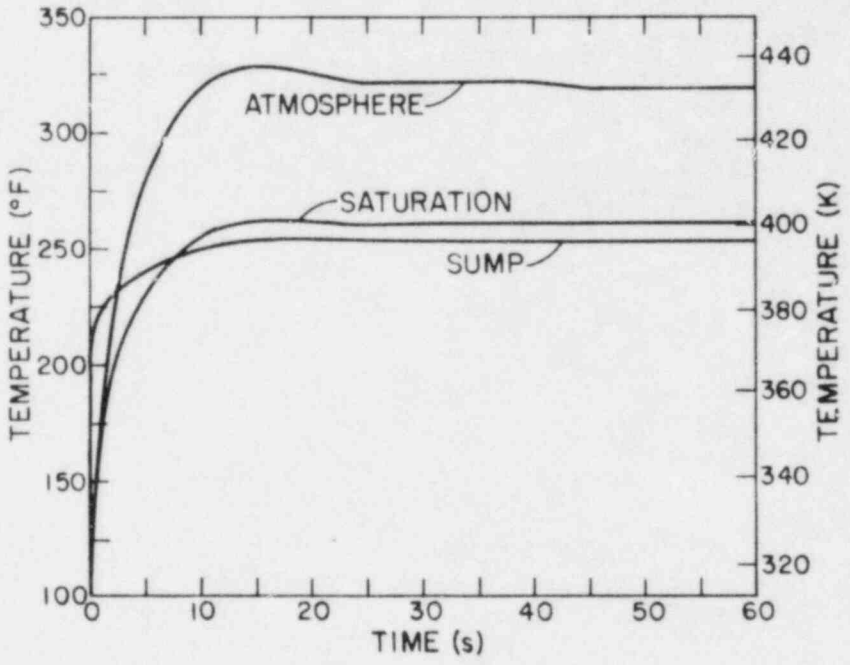

Fig. 5b. Temperatures vs time.

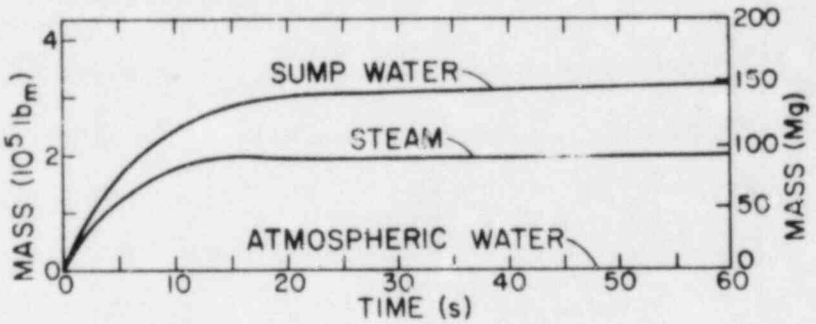

Fig. 5c. Water mass distribution vs time.

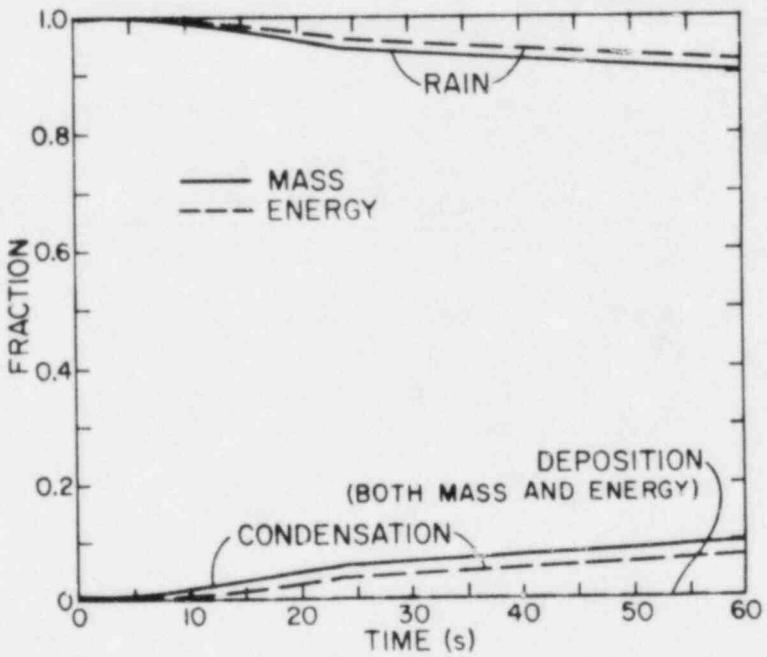

Fig. 5d. Sump mass and energy contribution fractions vs time.

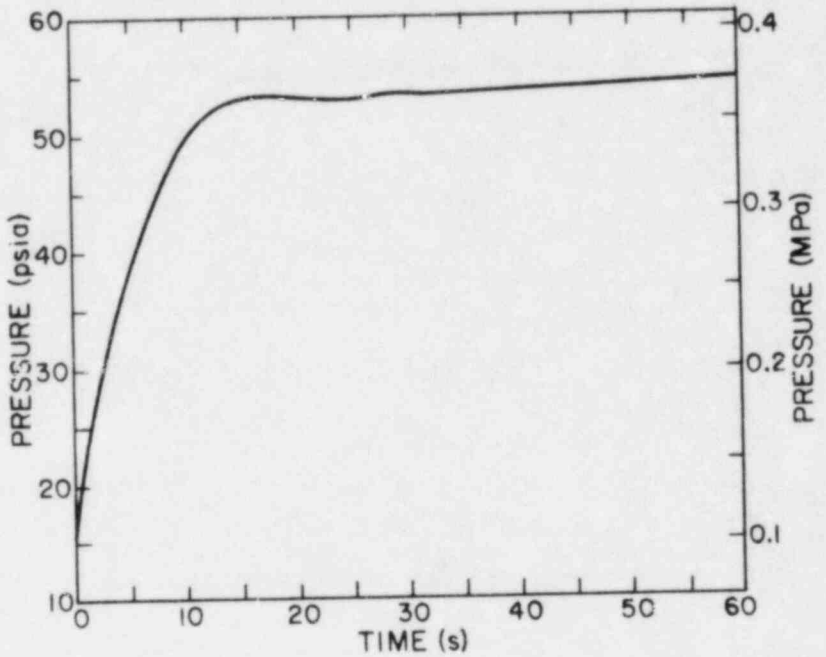

Fig. 6a. Mechanistic approach (M) calculated results for V_+ = 0.2 and drop diameter of 100 μm - Pressure vs Time.

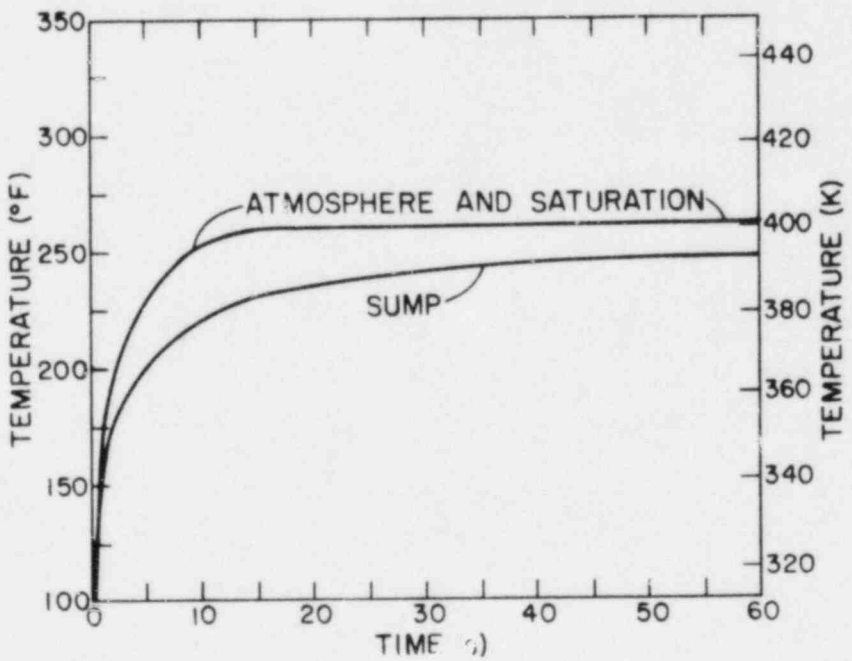

Fig. 6b. Temperatures vs time.

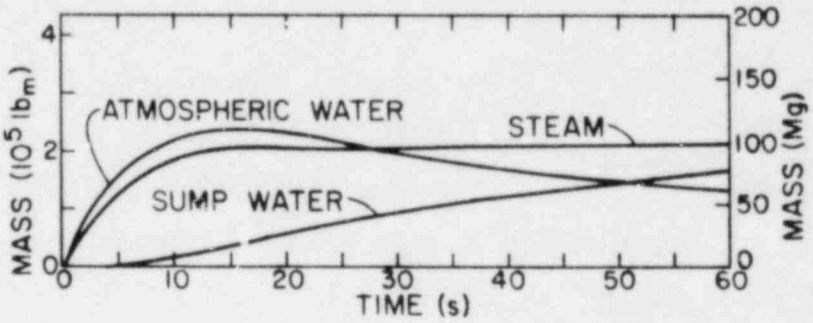

Fig. 6c. Water mass distribution vs time.

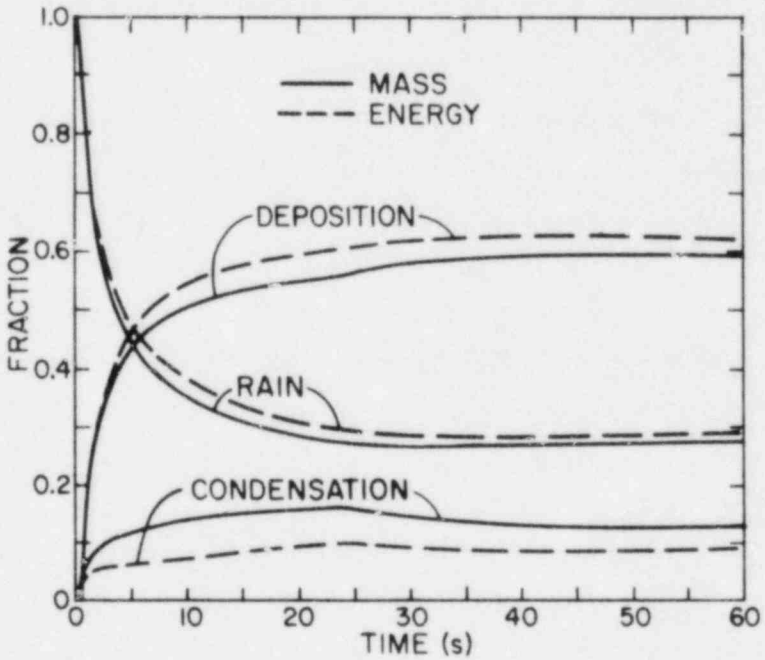

Fig. 6d. Sump mass and energy contribution fractions vs time.

1. Source temperature and mass removal[8] to be used in conjunction with condensation heat transfer.

2. Different partition models, see Table I.

3. Mechanistic model assumption variations, such as drop size and dimensionless drop deposition velocity (see Fig. 3).

A. Heat-Transfer Variations

Heat transfer to heat sinks within the containment is based on the Tagami[19] data, which are used to the end of blowdown, and Uchida[20] data, which are used after blowdown.* This approach is recommended by Refs. 24 and 25. These recommendations do not include consideration of the source temperature to be used and the resulting condensed mass. Reference 8 addressed these considerations and showed them to be important for a steam-line break analysis. This study resulted in the following recommendations for a main-steam-line-break containment analysis:

1. the difference between the bulk temperature and the wall temperature should be used to determine energy transfer to heat sinks and

2. the condensed mass to be associated with the energy transfer should be as given by Eq. (7).

In comparison, analyses have been previously performed with the steam saturation temperature used as the source temperature and the condensed mass associated with the heat transfer totally based on the latent heat of vaporization/condensation.[2]

Table III presents the results of this variation in performing the heat-transfer analysis. This comparison shows that the Ref. 8 recommendations resulted in small changes for the instantaneous mixing approach. However, the partition approach (S-P) is shown to be more sensitive. The difference of sensitivity is due to the differences in thermodynamic states. The I-R transient is mostly saturated whereas the S-P transient is mostly superheated. As discussed in Ref. 8, superheated steam temperature (and pressure) is quite sensitive to the steam specific internal energy, which is affected by the energy and mass removal caused by the heat transfer.

*See Appendix C.

TABLE III

SENSITIVITY (%) OF NEW HEAT-TRANSFER ASSUMPTION

Note: Sensitivity of parameter P = $(P_{new} - P_{old}) \times 100/P_{old}$ where old refers to the Ref. 2 assumptions ($T_{source} = T_{sat}$, mass removal based on h_{fg} only) and new refers to the Ref. 8 assumptions [$T_{source} = T_{bulk}$, mass removal based on Eq. (8)].

		Sensitivity (%)			
		Atmosphere		Sump	
Approach	Time, s	Pressure	Temp	Mass	Temp
Instantaneous Mixing with Rain (I-R)	20	0.4	0.4	- 0.4	- 1.4
	60	0.2	0.4	- 0.3	- 3.2
Representative Partition (S-P)	20	- 1.8	- 0.4	1.0	- 1.6
	60	- 3.3	- 2.7	2.2	- 1.9

B. Partition Approach Variations

Only a representative partition approach (S-P) was used for some of the previous comparisons. However, several partition approaches are proposed in Ref. 1 and summarized in Table I. Table IV summarizes the calculated results for the different partition approaches. These results are characterized by the early superheat temperature peak, which is due to the partition approaches introducing only vapor into the containment atmosphere. The results of Table IV are readily explained by considering the enthalpies of the vapor and liquid as they affect

1. the vapor temperature, and therefore pressure,
2. the sump temperature, and
3. the distribution of blowdown mass.

TABLE IV

DIFFERENT PARTITION APPROACH RESULTS

$$X = \frac{h_{in} - h_f}{h_g - h_f}$$

Designation	Partition Approach h_g	Partition Approach h_f	Time (s)	Atmosphere Pressure MPa	Atmosphere Pressure psia	Atmosphere Temp K	Atmosphere Temp °F	Sump Mass Mg	Sump Mass 10^5 lb$_m$	Sump Temp K	Sump Temp °F
P-P	Total Pressure	Total Pressure	10	0.389	56.4	456	360	108	2.37	370	206
			20	0.413	59.9	457	362	135	2.98	376	216
			60	0.403	58.5	451	352	144	3.18	377	218
S-P[a]	Steam Partial Pressure	Total Pressure	10	0.361	52.3	433	319	111	2.44	394	250
			20	0.386	56.0	436	325	138	3.04	397	254
			60	0.383	55.4	433	319	146	3.21	396	253
S-S	Steam Partial Pressure	Steam Partial Pressure	10	0.378	54.8	436	325	106	2.33	370	206
			20	0.405	58.8	440	332	132	2.92	375	215
			60	0.400	58.0	436	325	141	3.10	376	216
T-T	Atmosphere Temerature	Atmosphere Tempera-ture	10	0.369	53.5	448	347	112	2.48	397	254
			20	0.388	56.3	452	354	142	3.14	405	269[b]
			60	0.381	55.2	447	345	151	3.33	404	268[b]

[a] Representative Partition Approach used for other comparisons.

[b] Sump water temperature higher than atmosphere saturation temperature.

Note that we believe the blowdown is introduced into the containment as a dispersion of small drops. The partition approach is presented in recognition of its current use by others.

C. Mechanistic Approach Variations

The representative mechanistic model used in previous comparisons is based on a drop diameter (d) of 100 μm and a dimensionless deposition velocity (V_+) of 0.2. However, there are large uncertainties in the analyses leading to the drop-size estimates (Sec. II.A) and the deposition coefficients (Sec. II.B-D). It is important, therefore, to determine the effects of various values of d and V_+.

Tables V-VIII show the effects of various values of V_+ and d on calculated containment parameters. Tables V and VI show the effects on containment atmosphere pressure, temperature, and water mass. Table VII shows the effects on sump mass and temperature. Table VIII shows the effects on the fractions of the sump water that come from condensation, deposition, and rain.

Review of Tables V-VIII shows the following effects of the mechanistic approach drop diameters (d) and dimensionless deposition velocity (V_+) variation.

1. Atmosphere pressure is affected by 0.2% or less for the drop sizes (10-100 μm) estimated to be introduced by the blowdown (Ref. 7) and reasonable limits on V_+ of 0.1 to 0.4 (Tables V and VI).

2. Atmosphere temperature is not affected (Tables V and VI).

3. Water holdup in the atmosphere, and therefore sump mass, varies significantly, especially for the drop-size variation because of the increased rain for the large-size drops (Tables V through VIII).

4. Sump water temperature varies by only about $\pm$ 7 K ($\pm$ 13°F), Table VII. Note that the variation is directly dependent on the sump mass fraction. This is due to the condensate mass being at a different temperature (heat sink) than the rain mass, which is at the atmosphere temperature, and the deposition mass, which we have assumed to be at the atmosphere temperature (see Sec. II.C).

It should be noted that the lack of change in the calculated atmosphere temperature (and pressure because the atmosphere is saturated) is due to use of the same heat-transfer data for the determination of heat-sink energy removal. Actually, a variation in the deposited mass changes the heat transfer because

TABLE V

EFFECT OF MECHANISTIC APPROACH DROP DIAMETER (d) ON CALCULATED CONTAINMENT ATMOSPHERE CONDITIONS FOR FIXED DIMENSIONLESS DEPOSITION VELOCITY (V_+) OF 0.2

Notes: (1) Sensitivity (%) of pressure and temperature based on their values for different values of d relative to their values for d = 100 μm given in (2) below.

(2) Pressure and temperature for d = 100 μm and V_+ = 0.2 (See Fig. 3):
At 20 s - Pressure = 0.368 MPa (53.3 psia)
Temperature = 400 K (260°F)
At 60 s - Pressure = 0.376 MPa (54.5 psia)
Temperature = 401 K (262°F)

Drop Diameter (μm)	V_+	Sensitivity (%) Absolute Pressure 20 s	Absolute Pressure 60 s	Absolute Temperature 20 s	Absolute Temperature 60 s	Water Mass Fraction 20 s	Water Mass Fraction 60 s
1	0.2	- 0.2	- 0.2	0.0	0.0	0.401	0.305
10	0.2	- 0.2	- 0.2	0.0	0.0	0.401	0.304
100	0.2	0	0	0.0	0.0	0.386	0.261
500	0.2	0.4	0.4	0.0	0.0	0.301	0.082
1000	0.2	0.8	0.7	0.1	0.0	0.227	0.017

the liquid film thickness, velocity, and other parameters vary. This sophistication was not included in our analysis because the use of the Tagami/Uchida data is the current accepted practice, e.g., see Ref. 8. However, a more complete analysis of the heat transfer is a logical extension of the liquid film analyses that we have performed for the determination of mass deposition. This is recommended for future work.

TABLE VI

EFFECT OF MECHANISTIC APPROACH DIMENSIONLESS DEPOSITION VELOCITY (V_+) ON CALCULATED CONTAINMENT ATMOSPHERE CONDITIONS FOR FIXED DROP DIAMETER (d) of 100 μm

Notes: (1) Sensitivity (%) of pressure and temperature based on their values for different values of V_+ relative to their values for V_+ = 0.2 given in (2) below.

(2) Pressure and temperature for d = 100 μm and V_+ = 0.2 (see Fig. 3):
At 20 s - Pressure = 0.368 MPa (53.3 psia)
Temperature = 400 K (260°F)
At 60 s - Pressure = 0.376 MPa (54.5 psia)
Temperature = 401 K (262°F)

Dimensionless Deposition Velocity V_+	d(μm)	Sensitivity (%) Absolute Pressure 20 s	Absolute Pressure 60 s	Absolute Temperature 20 s	Absolute Temperature 60 s	Water Mass Fraction 20 s	Water Mass Fraction 60 s
0.4	100	0.2	0.2	0.0	0.0	0.333	0.138
0.2	100	-	-	-	-	0.386	0.261
0.1	100	- 0.2	- 0.2	0.0	0.0	0.405	0.326
0.02	100	- 0.2	- 0.2	0.0	0.0	0.416	0.369
0.002	100	- 0.2	- 0.2	0.0	0.0	0.416	0.369

TABLE VII

EFFECT OF MECHANISTIC APPROACH DROP DIAMETER (d) AND DIMENSIONLESS DEPOSITION VELOCITY (V_+) ON CALCULATED CONTAINMENT SUMP MASS AND TEMPERATURE

Drop Diameter d(μm)	Dimensionless Deposition Velocity V_+	Sump At 20 s Mass Mg	Mass 10^5 lbm	Temp K	Temp °F	At 60 s Mass Mg	Mass 10^5 lbm	Temp K	Temp °F
100	0.4	49	1.070	390	242	111	2.440	394	250
100	0.2	27	0.588	387	236	78	1.709	393	248
100	0.1	18	0.397	382	228	55	1.210	391	244
100	0.02	12	0.275	376	217	38	0.827	387	237
100	0.002	12	0.275	376	217	38	0.827	387	237
1	0.2	20	0.435	384	231	63	1.386	392	246
10	0.2	20	0.437	384	231	63	1.391	392	246
100	0.2	27	0.588	387	236	78	1.709	393	248
500	0.2	60	1.320	390	242	123	2.709	394	249
1000	0.2	83	1.827	391	243	135	2.976	393	247

TABLE VIII

EFFECT OF MECHANISTIC APPROACH DROP DIAMETER (d) AND DIMENSIONLESS DEPOSITION VELOCITY (V_+) ON CALCULATED SUMP MASS SOURCE FRACTIONS

Drop Diameter d(μm)	Dimensionless Deposition Velocity V_+	Sump Mass Source Fractions					
		Condensation		Deposition		Rain	
		20 s	60 s	20 s	60 s	20 s	60 s
100	0.4	0.09	0.09	0.77	0.77	0.14	0.14
100	0.2	0.16	0.13	0.55	0.59	0.29	0.28
100	0.1	0.24	0.18	0.32	0.36	0.44	0.46
100	0.02	0.34	0.27	0.0	0.0	0.66	0.73
100	0.002	0.34	0.26	0.0	0.0	0.66	0.74
1	0.2	0.22	0.16	0.78	0.84	0.0	0.0
10	0.2	0.22	0.16	0.78	0.84	0.0	0.0
100	0.2	0.16	0.13	0.55	0.59	0.29	0.28
500	0.2	0.07	0.08	0.18	0.19	0.75	0.73
1000	0.2	0.05	0.07	0.10	0.10	0.85	0.83

IV. CONCLUSIONS

1. The effects of blowdown-introduced drops on a dry-pressure-containment LOCA analysis can be estimated by a mechanistic approach.

2. The mechanistic approach depends on an accounting for the drop (particle) turbulent deposition and the drop deposition caused by gravity (rain), the latter based on terminal velocity.

3. To complete the mechanistic approach analysis, the effects of heat transfer (based on Tagami/Uchida data) and the associated condensed mass removal were included.

4. As a result of the drops, the atmosphere thermodynamic conditions were completely saturated.

5. Variation of the mechanistic approach assumptions results in small changes in the calculated atmosphere pressure and temperature. This is due to the use of the Tagami/Uchida heat-transfer data which have limited variations in, for example, film mass.

6. The film mechanics analyses developed for the estimation of mass transfer should be extended to the determination of heat transfer so that a more flexible heat-transfer model is available.

7. The mechanistic approach assumption variations had their primary effect on the atmosphere water retention and therefore the sump water mass.

8. Because of the large uncertainty in the estimated drop sizes and mass deposition velocity, these parameters were varied over a wide range in a sensitivity study of the mechanistic approach.

9. **In contrast to the approach of Ref. 2, which assumes instantaneous introduction of the blowdown and the raining of atmospheric liquid, the mechanistic approach results in significantly (5%) lower atmospheric pressure and slightly lower atmospheric temperature.**

10. In comparison with the partition approaches of Ref. 1, the mechanistic approach results in slightly (2%) lower atmospheric pressure and significantly lower atmospheric temperature.

APPENDIX A

DROP DEPOSITION ON A FALLING LIQUID FILM BY ANALOGY

The purpose of this appendix is to evaluate the drop mass deposition correlation depicted in Fig. 2 by the derivation of a drop mass deposition relationship based on the analogy between drop mass and momentum transfer. The advantage of using the analogy (Ref. 26) is that the better understood mechanics of momentum transfer can be modified by a simple factor to obtain the not so readily measured drop mass transfer. The factor used is the ratio of drop mass eddy diffusivity (ε_d) to momentum eddy diffusivity (ε), which becomes the connecting link between drop mass and momentum transfer.

The drop mass-transfer rate can be expressed by

$$m_d = (D_d + \varepsilon_d) \frac{dC}{dy} + u_t C \,, \tag{A-1}$$

where D_d is the Brownian drop mass diffusivity, ε_d is the drop mass eddy diffusivity, C is the drop mass concentration, y is the normal-to-the-wall coordinate, and u_t is the drop equilibrium (terminal) velocity resulting from a drop body force, such as gravity, which for a vertical containment surface is zero. The Brownian drop mass diffusivity is given by (Ref. 27)

$$D_d = \frac{K'T}{3\pi\mu d} \,, \tag{A-2}$$

where K' is Boltzmann's constant, T is absolute temperature, μ is the gas viscosity, and d is drop diameter.

Equation (A-1) will now be applied to a containment vertical wall with a falling liquid film as shown in Fig. A.1. The liquid is a result of condensation and drop mass deposition and is assumed to form a wavy interface because of the large heights involved in containments. The figure shows the film wave height B, the mean film velocity u_δ, and a wave crest velocity of u_c. Between the liquid film and the bulk atmosphere a boundary layer of thickness Δ is shown. In this boundary layer, the drop mass concentration diminishes from the bulk value C_b to zero at the liquid film. In

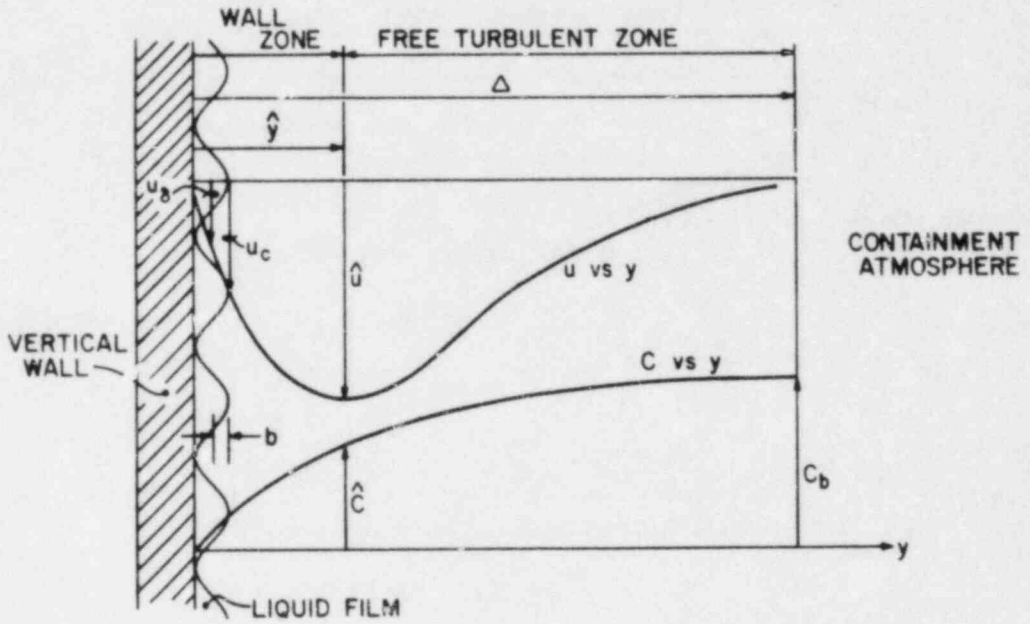

Fig. A.1. Schematic representation of the falling liquid film and steam-air-liquid drop boundary layer that is between the containment atmosphere and a vertical heat sink.

addition, we have assumed that the boundary layer velocity has a free-turbulent and a wall zone separated where the downward velocity is a maximum ($\hat{u}$). Because of the wavy surface, a turbulent film can be assumed resulting in $\varepsilon_d >> D_d$. Equation (A-1) becomes, with $u_t = 0$,

$$m_d = \varepsilon_d \frac{dC}{dy} \quad .$$

Introducing the diffusivity ratio into this equation results in

$$m_d = \frac{\varepsilon_d}{\varepsilon} \varepsilon \frac{dC}{dy} \quad . \tag{A-3}$$

We will now develop an approximate expression for ε for substitution into Eq. (A-3) based on Prandtl's mixing length and Karman's similarity theories (Ref. 28). Assuming isotropic turbulence,

$$\varepsilon = u'\ell \quad , \tag{A-4}$$

where u' is the mean turbulent velocity fluctuation and the mixing length ℓ is given by

$$\ell = K y \quad , \tag{A-5}$$

which applies to either a smooth or rough interface (Note, Ref. 28, pg. 510, shows that $K \simeq 0.4$). In addition, we can use

$$u' = \ell \frac{du}{dy} \quad . \tag{A-6}$$

Substitution of Eqs. (A-5) and (A-6) into Eq. (A-4) gives

$$\varepsilon = (K y)^2 \frac{du}{dy} \quad . \tag{A-7}$$

To obtain the du/dy term in Eq. (A-7), we will use the logarithmic velocity distribution law for a rough surface from Ref. 28.

$$\frac{u}{V_\star} = \frac{1}{K} \ln \frac{y}{B} + S \quad , \tag{A-8}$$

where $V_\star$ is the interfacial shear stress or friction velocity, B is the roughness height (in this case the wave height), and S is a constant. The shear stress velocity is related to the interface shear stress τ and density ρ by

$$V_\star = \sqrt{\frac{\tau}{\rho}} \quad . \tag{A-9}$$

When the interface is "hydraulically rough," the shear stress at the interface depends on the local velocity and not on the peak velocity $\hat{u}$. This can be deduced from Eq. (A-8) by substituting $u = u_c$ at $y = B$, which results in

$$S = \frac{u_c}{B} \quad . \tag{A-10}$$

Substitution of Eq. (A-10) into Eq. (A-8) results in

$$\frac{u}{V_*} = \frac{1}{K} \ln \frac{y}{B} + \frac{u_k}{V_*} \quad . \tag{A-11}$$

Differentiation of Eq. (A-11) gives

$$\frac{du}{dy} = \frac{V_*}{K y} \quad ,$$

which can be substituted into Eq. (A-7) to produce

$$\varepsilon = K y V_* \quad . \tag{A-12}$$

Comparison of Eq. (A-12) with Eqs. (A-4) and (A-5) reveals that $V_* = u'$, which approximately agrees with measurements (Ref. 29). Substituting Eq. (A-12) into Eq. (A-3) results in

$$m_d = \frac{\varepsilon_d}{\varepsilon} K y V_* \frac{dC}{dy} \quad . \tag{A-13}$$

To complete the development sought, we will use

1. $\beta_d = m_d/C_b$, where β_d is the drop mass-transfer coefficient,

2. $V_+ = \beta_d/V_*$, where V_+ is the dimensionless particle (drop) deposition velocity used in Fig. 3.

3. $(K y)_{avg.} \simeq K \hat{y}/2$, see Fig. A.1,

4. $dC/dy = \hat{C}/\hat{y}$ for the wall zone shown in Fig. A.1, and

5. $(\hat{C}/C_b) = (\hat{y}/\Delta)^{1/7}$ based on a 1/7 concentration profile.

Substitution of the above into Eq. (A-13) results in

$$V_+ = \frac{\beta_d}{V_*} = \frac{\varepsilon_d}{\varepsilon} \frac{K}{2} \left(\frac{y}{\Delta}\right)^{1/7} \quad . \tag{A-14}$$

The value of K = 0.4 can be used based on the classic mixing analysis approach (Ref. 28, pg. 510). Also, our application of the same approach to the boundary layer shown in Fig. A.1 gave $\hat{y}/\Delta = 0.061$. Substitution of these values gives

$$V_+ = 0.134 \frac{\varepsilon_d}{\varepsilon} \quad . \tag{A-15}$$

To complete the analysis of this appendix, values of $\varepsilon_d/\varepsilon$ are needed. A literature search of deposition and diffusion measurements for fuel sprays revealed that $\varepsilon_d/\varepsilon$ values ranged between 1 and 2. Substitution of these eddy diffusivity ratios into Eq. (A-15) gives V_+ values between 0.134 and 0.268. These values bracket the maximum value of V_+ in Fig. 2 and therefore give us confidence in using Fig. 3.

APPENDIX B

INTERFACIAL SHEAR STRESS

The deposition section in the main text of this report suggests the use of the deposition correlation presented in Fig. 3 for the determination of drop mass deposition. However, the use of this correlation requires the interfacial shear stress (friction) velocity term V_*. In this appendix we will develop and verify that an appropriate expression is

$$V_* = u_\delta/10 \ , \tag{B-1}$$

where u_δ is the mean velocity of the falling liquid film, $V_* = \sqrt{\tau/\rho_g}$, τ is the interfacial shear, and ρ_g is the gas density near the interface.

We will now develop a relationship for the interfacial shear stress. This is for a liquid film that is falling on a vertical wall, see Fig. 1. According to experimenters "falling films" rarely have smooth interfaces. In laminar flow a rippled interface persists to Reynolds number as low as 6. When turbulence sets in, the wave structure become increasingly complex as the Reynolds number is increased. It becomes obvious that the "roughness" of the interface is a significant factor in determining the flow stresses. For example, Schlichting (Ref. 28) in his early work measured the shear stress over various types of roughness elements in terms of u_c/V_*, where u_c is the fluid velocity immediately over the crests of the roughness elements. A similar relationship can be developed for roughness associated with a following liquid film.

Chien[17] carefully measured the liquid film structure for a "falling film" and for films in annular two-phase flow. Measurements of pressure drop, wave crest height, mean film thickness, and continuous sublayer thickness were made. Chien's two-phase low data are successfully correlated by relating the superficial friction factor (f'_g) to the disturbed liquid film thickness ($\delta_m - \delta_B$) by

$$f'_g = 1.2 \left(\frac{\delta_m - \delta_B}{D} \right)^{0.485} \ , \tag{B-2}$$

where D is the experimental tube diameter, δ_m is the mean film thickness, and

δ_B is the minimum film thickness (Fig. B.1). Shear stress can be introduced into Eq. (B-2) by means of

$$f'_g = \frac{8\,\tau}{\rho_g\, V'^2_g}\,, \tag{B-3}$$

where τ is the shear stress, ρ_g is the gas density near the interface, and V'_g is the superficial gas velocity. Equations (B-2) and (B-3) can be used to obtain the shear stress, needed in Eq. (B-1), in terms of the superficial velocity.

To obtain the Eq. (B-1) expression, u_δ must be related to the superficial velocity. This can be done via the velocity profile for a rough wall with u_δ, the velocity on the profile at the mean film thickness distance from the wall. Note that we have assumed that the mean film velocity is approximately equal to the gas velocity u_c at the interface. This is shown to be a good assumption in the following verification discussion.

Application of the above procedures(to Chien's data)results in the $u_\delta/V_\star$ vs liquid film Reynolds correlation given in Table B-I. The resulting correlation shows that $u_\delta/V_\star$ is relatively constant (at a value of about 10) over a wide range of liquid film Reynolds numbers. This is not surprising considering that the turbulent friction factor for a rough surface is relatively independent

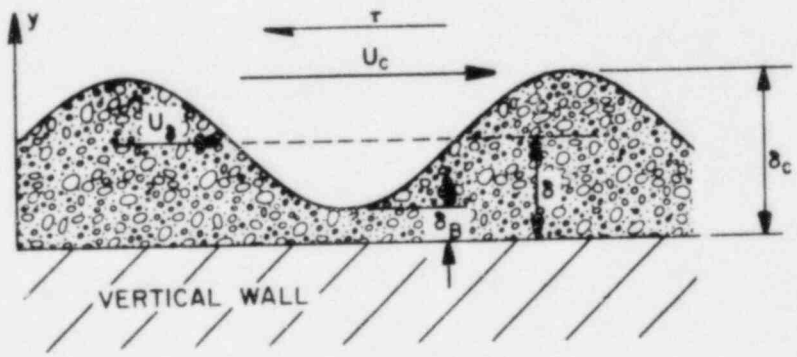

Fig. B.1. Schematic representation of falling liquid film.

TABLE B-I

REDUCTION OF CHIEN'S (Ref. 17) FALLING LIQUID FILM MEASUREMENTS TO A CORRELATION BETWEEN THE RATIO OF MEAN LIQUID FILM VELOCITY (u_δ) AND INTERFACE SHEAR STRESS VELOCITY ($V_\star$)

Test Run	Liquid Mass Flow (kg/s/m)	Liquid Film Reynolds No.	Film Geometry (see Fig. B.1) mm δ_c	δ	δ_B	u_δ (m/s)	$\frac{u_\delta}{V_\star}$
1	0.287	338	2.16	0.81	0.66	0.41	9.6
2	0.958	1128	4.06	0.94	0.66	1.17	10.2
3	1.758	2068	5.08	1.07	0.66	1.89	10.4
4	2.700	3177	6.10	1.27	0.66	2.44	10.2
5	3.781	4450	7.11	1.65	0.66	2.63	10.1

of Reynolds number. Similar results are reported in Ref. 30. To verify the experimentally indicated $u_\delta/V_\star$ value of about 10, two theoretically based estimates of this ratio are now given. The first uses Prandtl's mixing length hypothesis for an idealized wave structure, and the second uses the Blasius shear equation for turbulent flow between the wave crests.

1. Prandtl's Mixing Length Hypothesis. Figure B.2 depicts an idealized wavy liquid film with a wave amplitude (b) equal to its mean thickness δ. Note that the liquid film and gas velocity profiles are assumed to be approximately identical. This defines the gas velocity at several points to be used with the Prandtl's mixing length hypothesis (Ref. 28)

$$\tau = \rho \ell^2 \left|\left(\frac{du}{dy}\right)_w\right| \left(\frac{du}{dy}\right)_w , \qquad \text{(B-4)}$$

where τ is the wall (or interfacial shear stress, approximately), ρ is the gas density near the interface, ℓ is the mixing length, and $(du/dy)_w$ is a representative velocity gradient near the wall. From Ref. 28, $\ell = Ky$, where $K = 0.4$, a universal constant for turbulent flow. Equation (B-4) then becomes

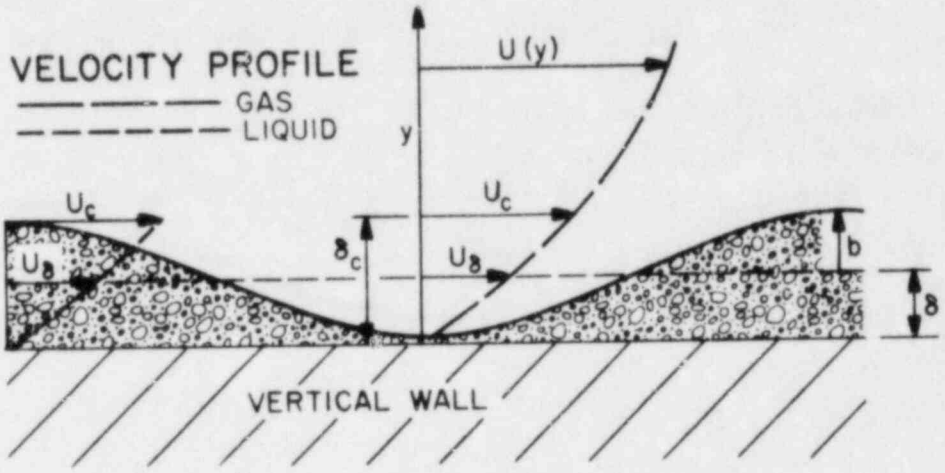

Fig. B.2. Schematic representation of an idealized liquid film for Prandtl's mixing length hypothesis application (note identical liquid and gas velocity profiles).

$$\tau = \rho K^2 y^2 \left(\frac{du}{dy}\right)_w^2$$

or

$$V_* = Ky\left(\frac{du}{dy}\right)_w \quad . \tag{B-5}$$

Let us assume that the velocity gradient in Eq. (B-5) at y = b is

$$\frac{u_c - u_\delta}{b} \quad .$$

As a result, Eq. (B-5) becomes

$$V_* = 2K(u_c - u_\delta) = 2K\, c_R \quad , \tag{B-6}$$

where $c_R = u_k - u_\delta$ is the velocity of propagation of a wave relative to its undisturbed fluid, which is flowing at the velocity u_δ as shown in Fig. B.3.

We now need suitable values for substitution into Eq. (B-6). References 31 and 32 indicate that a suitable value for c_R/u_δ is 0.12 (for a water film in contact with air). Also, K = 0.4. Substitution results in

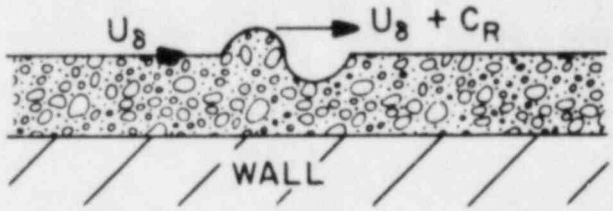

Fig. B.3. Disturbance wave propagation velocity is c_R greater than film velocity (u_δ).

$$\frac{u_\delta}{V_\star} \simeq 10.4 \ ,$$

which is close to that obtained from Chien's data as shown in Table B-I. Note that the assumption that $u_\delta \simeq u_c$ is confirmed by the small value of c_R, which is for a small amplitude wave and therefore of questionable applicability to the present situation. In fact,

$$\frac{C_R}{u_\delta} = 0.12 = \frac{u_c}{u_\delta} - 1$$

results in $u_c/u_\delta = 1.12$.

2. Blasius Shear Stress. The Balsius shear stress equation is

$$\tau = 0.0228 \, \rho \, u^2 \left(\frac{\nu}{uy}\right)^{1/4} .$$

Based on Figs. B.1 and B.2, we will assume the equation can be applied at $y = y' = \delta - \delta_b$, at which the gas velocity is assumed to be equal to the liquid velocity u_δ. As a result,

$$V_\star^2 = \tau/\rho = 0.0228 \, u_\delta^2 \left(\frac{\nu}{u_\delta \, \delta}\right)^{1/4} . \qquad \text{(B-7)}$$

Substituting the $u_c/u_\delta = 1.12$ value developed in Sec. 1 above, the kinematic viscosity for air, and the $(\delta - \delta_B)$ values from Table B-I into Eq. (B-7), results in $u_c/V_\star$ values ranging from 9.5 to 14.1 for Runs 1 through 5, respectively,

of Chien's data. These values are reasonably close to those in Table B-I, although somewhat higher, which may be due to real wave structure being rougher than that assumed in the idealized model.

APPENDIX C

CONTAINMENT PROBLEM

The dry pressure containment calculations performed for LOCA analysis are based on the representative problem described by the (1) basic parameters of Table C-I, (2) LOCA blowdown of Table C-II, and (3) passive heat sinks described by Tables C-III and C-IV. Note that the heat-sink description uses (1) a liner-to-concrete contact resistance of 57 $W/m^2/K$ (10 $Btu/h/ft^2/^oF$) and (2) a concrete thickness of only ~0.15 m (6 in.), which are recommended in Ref. 33.

Heat transfer to heat sinks within the containment, except for the containment floor/sump region, is based on the Tagami[19] and Uchida[20] condensation heat-transfer data. The Tagami data are used to the end of blowdown after which the Uchida data are used. Heat transfer from the containment atmosphere to the containment floor/sump region is based on a coefficient of 1.1 $W/m^2/K$ (0.2 $Btu/h/ft^2/^oF$). Heat transfer to the sump liquid is assumed to be negligible.

Calculations were performed with the COMPARE-Mod 1 code[23] modified to include (1) a sump, (2) drop deposition, (3) terminal-velocity precipitation, and (4) various partition approaches, etc. The acceptability of the COMPARE (a containment subcompartment analysis) code to perform containment pressure-temperature analysis was verified by comparing results for identical calculations with the COMPARE and CONTEMPT (Ref. 2) codes.

TABLE C-I

CONTAINMENT PROBLEM BASIC PARAMETERS

Net Free Internal Volume, m^3 (ft^3) - 7.02×10^4 (2.48×10^6)

Initial Absolute Total Pressure, MPa (lb_f/m^2) - 0.101 (14.7)

Initial Temperature, K (^oF) - 319. (115.)

Initial Relative Humidity, percent - 30

End of Blowdown Time, s - 20.5

Spray Initiation Time, s - 60.

TABLE C-II

CONTAINMENT PROBLEM LOCA BLOWDOWN

	Mass-Flow Rate		Energy-Flow Rate		Enthalpy	
Time,s	Mg/s	$10^3 lb_m/s$	GJ/s	10^6Btu/s	MJ/kg	Btu/lb_m
0.	0.	0.	0.	0.	--	--
0.025	34.81	76.75	45.93	43.56	0.5988	567.6
0.075	34.24	75.51	45.23	42.90	0.5993	568.1
0.2	36.16	79.73	47.95	45.48	0.6018	570.4
0.25	43.45	95.82	57.75	54.78	0.6031	571.7
0.5	40.24	88.74	54.04	51.26	0.6094	577.6
1.0	36.30	80.04	49.78	47.22	0.6225	590.0
1.2	30.34	66.91	41.58	39.44	0.6218	589.4
2.0	24.58	54.19	33.59	31.86	0.6202	587.9
4.0	19.94	43.97	27.54	26.12	0.6267	594.0
6.0	14.51	31.99	22.98	21.80	0.7190	681.5
10.0	8.961	19.76	13.56	12.86	0.6866	650.8
13.5	4.150	9.151	5.298	5.025	0.5793	549.1
15.0	2.408	5.309	2.925	2.774	0.5512	522.5
15.2	2.276	5.018	2.733	2.592	0.5449	516.5
15.5	2.669	5.885	3.063	2.905	0.5207	493.6
16.5	2.135	4.708	2.450	2.324	0.5207	493.6
17.5	1.601	3.531	1.838	1.743	0.5207	493.6
18.5	1.067	2.353	1.225	1.162	0.5210	493.8
19.5	0.533	1.176	0.613	0.581	0.5212	494.0
20.5[a]	0.	0.	0.	0.	--	--
23.0	0.226	0.498	0.682	0.647	1.371	1299.
24.5	0.314	0.693	0.950	0.901	1.372	1300.
26.0	0.373	0.823	1.131	1.073	1.376	1304.
26.3	0.187	0.412	0.564	0.535	1.370	1298.
40.0	0.182	0.401	0.549	0.521	1.371	1299.
50.0	0.178	0.393	0.538	0.510	1.370	1298.
60.0	0.174	0.384	0.527	0.500	1.374	1302.
69.7	0.171	0.376	0.516	0.489	1.372	1300.
70.0	0.340	0.750	1.031	0.978	1.376	1304.

[a]End of blowdown.

TABLE C-III

CONTAINMENT PROBLEM HEAT SINKS

Heat Sink, Area, and Composition	Thickness mm	Thickness in.
Containment Wall [6 638 m^2 (72 450 ft^2)]	1073.	42.256
Inorganic coating	0.15	0.006
Carbon steel liner plate[a]	6.35	0.25
Concrete[a]	165.1	6.5
Containment Dome [2 244 m^2 (24 150 ft^2)]	768.50	30.256
Inorganic coating	0.15	0.006
Carbon steel liner plate[a]	6.35	0.250
Concrete[a]	165.1	6.5
Thick Steel [307 m^2 (3 300 ft^2)]	50.95	2.006
Inorganic Coating	0.15	0.006
Carbon steel	50.8	2.000
Thin Steel [2 343 m^2 (25 220 ft^2)]	9.04	0.356
Inorganic coating	0.15	0.006
Carbon steel	8.89	0.350
Unlined Concrete Partitions [4 942 m^2 (53 200 ft^2)]	457.2	18.0
Concrete	165.1	6.5
Stainless Steel Lined Concrete [990 m^2 (10 660 ft^2)]	616.0	24.25
Stainless steel [a]	6.35	0.25
Concrete [a]	165.1	6.5
Containment Floor/Sump Region [1 308 m^2 (14 080 ft^2)]	1832.2	72.135
Organic coating	3.43	0.135
Concrete	165.1	6.5

[a]Contact resistance between steel and concrete.

TABLE C-IV

CONTAINMENT PROBLEM HEAT-SINK THERMAL PROPERTIES

Material	Thermal Conductivity W/m/K	Thermal Conductivity Btu/h/ft^2/^{o}F	Density Mg/m^3	Density lb$_m$/ft^3	Constant Press. Specific Heat J/kg/K	Constant Press. Specific Heat Btu/lb$_m$/^{o}F
Organic coating	0.17	0.1	1.51	94.	1381.	0.33
Inorganic coating	1.7	1.0	2.72	170.	502.	0.12
Stainless steel	17.	10.0	7.85	490.	460.	0.11
Carbon steel	43.3	25.0	7.85	490.	460.	0.11
Concrete	1.4	0.8	2.29	143.	879.	0.21

REFERENCES

1. R. C. Mitchell, "Description of the CONTRANS Digital Computer Code for Containment Pressure and Temperature Transient Analysis," Combustion Engineering report CENPD-140-A (April 1974, Reissue June 1976).

2. D. W. Hargroves, "CONTEMPT-LT/028 - A Computer Program for Predicting Containment Pressure-Temperature Response to a Loss-of-Coolant Accident," EG&G Idaho, Inc. report TREE-1279 (March 1979).

3. K. K. Almenas and J. M. Marchello, "The Physical State of Post-Loss-of-Coolant Accident Containment Atmospheres," ANS Nucl. Tech. 44, 411-428 (August 1979).

4. R. G. Gido and D. E. Lamkin, "Containment Main Steam Line Break Equipment Qualification," ANS Trans 44, 501-053 (November 1979).

5. R. G. Gido and A. Koestel, "LOCA Generated Drop Size Prediction - A Thermal Fragmentation Model," ANS 1978 Winter Mtg., Washington, DC (November 12-17, 1978).

6. A. Koestel, R. G. Gido, and J. S. Gilbert, "Film Entrainment and Drop Deposition for Two-Phase Flow," ANS/ASME Nuclear Reactors Thermal-Hydraulic Topical Meeting, Saratoga, NY (October 6-10, 1980).

7. A. Koestel and R. G. Gido, "LOCA Drop Size Estimates," Los Alamos Scientific Laboratory report NUREG/CR-1607, LA-8449-MS (August 1980).

8. D. E. Lamkin, A. Koestel, R. G. Gido, and P. W. Baranowsky, "Containment Main Steam Line Break Analysis for Equipment Qualification," Los Alamos Scientific Laboratory report NUREG/CR-1511, LA-8305-MS (June 1980).

9. P. Hutchinson, G. F. Hewitt, and A. E. Dukler, "Deposition of Liquid or Solid Dispersions from Turbulent Gas Streams: A Stochastic Model," J. Eng. Science 26, 419-439 (1971).

10 Combustion Processes, V. II, High Speed Aerodynamics and Jet Propulsion, Sec. J (Princeton University Press, 1956).

11. P. O. Rouhianian and J. W. Stachiewicz, "On the Deposition of Small Particles from Turbulent Streams," Trans. of the ASME, J. of Heat Transfer (February 1970).

12. B. Y. Liu and J. K. Agrawal, Experimental Observations of Aerosol Deposition in Turbulent Flow, V. 5 (Aerosol Science, Pergamon Press, 1974).

13. L. B. Cousins and G. F. Hewitt, "Liquid Phase Mass Transfer in Annular Two-Phase Flow: Droplet Deposition and Liquid Entrainment," Atomic Energy Research Establishment report R5657, Harwell, Berkshire, United Kingdom (1968).

14. E. N. Ganić and W. M. Rohsenow, "On the Mechanism of Liquid Drop Deposition in Two-Phase Flow," Trans. ASME 101, 288-294 (May 1979).

15. H. E. Hesketh, Fine Particles in Gaseous Media (Ann Arbor Science Publishers, 19.7).

16. C. T. Crowe, "Vapor - Droplet Flow Equations," Lawrence Livermore Laboratory report UCRL-51877 (August 1975).

17. S. F. Chien, "An Experimental Investigation of the Liquid Film Structure and Pressure Drop of Vertical, Downward, Annular, Two-Phase Flow," U. of Minn., Ph.D. Thesis (1961).

18. W. M. Rohsenow and H. Y. Choi, Heat, Mass and Momentum Transfer (Prentice-Hall, 1961).

19. T. Tagami, "Interim Report on Safety Assessments and Facilities Establishment Project in Japan for Period Ending June 1965 (No. 1)," Unpublished work (February 28, 1966).

20. H. Uchida, A. Oyama, and T. Togo, "Evaluation of Post Incident Cooling Systems of Light-Water Power Reactors," in Proceedings of the Third International Conference on the Peaceful Uses of Atomic Energy, Geneva (August 31-September 9, 1964) V. 13 (A/Conf. 28/10/436)(May 1964) pp. 93-104, United Nations (1965).

21. R. Clift, J. R. Grace and M. E. Weber, Bubbles, Drops and Particles, (Academic Press, 1978).

22. D. Bharathan, H. J. Richter, G. B. Wallis, and A. Akuffo, "An Investigation of the Distribution and Entrainment of ECC Water Injected into the Upper Plenum," Thayer School of Eng., Dartmouth College report NUREG/CR-1078 (January 1980).

23. R. G. Gido, J. S. Gilbert, R. G. Lawton, and W. L. Jensen, "COMPARE-Mod 1: A Code for the Transient Analysis of Volumes with Heat Sinks, Flowing Vents, and Doors," Los Alamos Scientific Laboratory report LA-7199-MS (March 1978).

24. "Standard Review Plan for the Review of Safety Analysis Reports for Nuclear Power Plants," Sec. 6.2.1.2. Office of Nuclear Reactor Regulation, US Nuclear Regulatory Commission report NUREG-75/087, LWR edition (September 1975).

25. D. C. Slaughterbeck, Review of Heat Transfer Coefficients for Condensing Steam in a Containment Building following a Loss-of-Coolant Accident," Idaho Nuclear Corp. report IN-1388 (September 1970).

26. E. R. Eckert and R. M. Drake, Jr., Analysis of Heat and Mass Transfer (McGraw-Hill Book Co., 1972) pp. 741-742.

27. A. Einstein, Annals of Physics (Vol. 17, pp. 549-560, 1905).

28. H. Schlichting, Boundary Layer Theory, 4th (McGraw-Hill Book Co., 1960).

29. P. Hutchinson, G. F. Hewitt, and A. E. Dunkler, "Deposition of Liquid or Solid Dispersions from Turbulent Gas Streams: A Stochastic Model," J. Eng. Science 26, 419-439 (1971).

30. H. Schlicting, "Experimental Investigation of the Problem of Surface Roughness," NACA Tech. Mem. No. 823, Trans. from Ing-Arch. V7, pp. 1-34 (1936).

31. S. Feldman, "On the Hydrodynamic Stability of Two Viscous, Incompressible Fluids in Parallel Uniform Shearing Motion," J. of Fluid Mechanics (1957).

32. S. Ostrach and A. Koestel, "Film Instabilities in Two-Phase Flow," AIChE J.(March 1965).

33. R. G. Gido, "Liner-Concrete Heat Transfer Study for Nuclear Power Plant Containments," Los Alamos Scientific Laboratory report LA-7089-MS (January 1978).

DISTRIBUTION

	Copies
Nuclear Regulatory Commission, R4, Bethesda, Maryland	333
Technical Information Center, Oak Ridge, Tennessee	2
Los Alamos National Laboratory, Los Alamos, New Mexico	50
	385

NRC FORM 335 (11-81)

U.S. NUCLEAR REGULATORY COMMISSION

BIBLIOGRAPHIC DATA SHEET

1. REPORT NUMBER (Assigned by DDC)
NUREG/CR-2848
LA-9460-MS

4. TITLE AND SUBTITLE (Add Volume No., if appropriate)
Mechanistic Dry-Pressure-Containment LOCA Analysis

2. (Leave blank)

3. RECIPIENT'S ACCESSION NO.

7. AUTHOR(S)
R. Gido, D. Lamkin, and A. Koestel

5. DATE REPORT COMPLETED
MONTH: June YEAR: 1982

9. PERFORMING ORGANIZATION NAME AND MAILING ADDRESS (Include Zip Code)
Los Alamos National Laboratory
P. O. Box 1663
Los Alamos, NM 87545

DATE REPORT ISSUED
MONTH: January YEAR: 1983

6. (Leave blank)

8. (Leave blank)

12. SPONSORING ORGANIZATION NAME AND MAILING ADDRESS (Include Zip Code)
Division of Systems Integration
Office of Nuclear Reactor Regulation
U. S. Nuclear Regulatory Commission
Washington, DC 20555

10. PROJECT/TASK/WORK UNIT NO.

11. FIN NO.
FIN A7105

13. TYPE OF REPORT
Technical

PERIOD COVERED (Inclusive dates)

15. SUPPLEMENTARY NOTES

14. (Leave blank)

16. ABSTRACT (200 words or less)

Procedures for performing mechanistic dry-pressure-containment LOCA analyses are presented, evaluated, applied and compared with other approaches. The procedures are based on (1) the blowdown-introduced small drops (10 to 100 um) being homogeneously mixed into the atmosphere, (2) drop (particle) turbulent deposition on vertical surfaces, and (3) terminal velocity gravity deposition on the floor. Variation of drop size and mass tranfer deposition velocity was found to have a small effect on calculated results, except for the atmosphere water mass retention. The primary effect of the mechanistic approach was a saturated containment atmosphere, with significant atmosphere water retention. The calculated containment pressure of the mechanistic approach was lower, before the spray initiation, than that calculated by other current procedures.

17. KEY WORDS AND DOCUMENT ANALYSIS

17a. DESCRIPTORS

17b. IDENTIFIERS/OPEN-ENDED TERMS

18. AVAILABILITY STATEMENT
Unlimited

19. SECURITY CLASS (This report)
Unclassified

21. NO. OF PAGES

20. SECURITY CLASS (This page)
Unclassified

22. PRICE
$

NRC FORM 335 (11-81)

UNITED STATES
NUCLEAR REGULATORY COMMISSION
WASHINGTON, D.C. 20555

FOURTH CLASS MAIL
POSTAGE & FEES PAID
USNRC
WASH D C
PERMIT No G-67

NUREG/CR-2848